Quantum control-enhanced sensing and spectroscopy with NV qubits in diamond

PROCEEDINGS OF SPIE

SPIEDigitalLibrary.org/conference-proceedings-of-spie

Quantum control-enhanced sensing and spectroscopy with NV qubits in diamond

Hernández-Gómez, S., Poggiali, F., Cappellaro, P., Fabbri, N.

S. Hernández-Gómez, F. Poggiali, P. Cappellaro, N. Fabbri, "Quantum control-enhanced sensing and spectroscopy with NV qubits in diamond," Proc. SPIE 11091, Quantum Nanophotonic Materials, Devices, and Systems 2019, 110910L (3 September 2019); doi: 10.1117/12.2531734

SPIE.

Event: SPIE Nanoscience + Engineering, 2019, San Diego, California, United States

Invited Paper

Quantum control-enhanced sensing and spectroscopy with NV qubits in diamond

S. Hernández-Gómez[a], F. Poggiali[a], P. Cappellaro[b], and N. Fabbri[a]

[a]European Laboratory for Non-linear Spectroscopy (LENS) and Department of Physics, Università degli Studi di Firenze, and Istituto Nazionale di Ottica del Consiglio Nazionale delle Ricerche (CNR-INO), I-50019 Sesto Fiorentino, Italy
[b]Department of Nuclear Science and Engineering, Massachusetts Institute of Technology, Cambridge, MA 02139

ABSTRACT

Quantum sensors take advantage of the inherent sensitivity of quantum systems to external environment perturbations to precisely measure target signals. The same interaction with the environment, however, limits the device sensitivity by reducing the coherence of the quantum states. Quantum control can play a crucial role in improving the sensor performance. We explore quantum control tools to improve the performance of a Nitrogen-Vacancy (NV) center as a single-qubit sensor of ultra-weak magnetic fields in noisy environments. We present a method to obtain a precise spectroscopic characterization of the NV environment, instrumental to design robust sensing strategies with improved noise protection. Then, we exploit *optimal quantum control* — based on a set of numerical methods to optimize the temporal dependence of the sensor driving field — adapted to quantum sensing purposes, and prove its advantage to achieve best compromises between signal acquisition and noise cancellation.

Keywords: NV centers in diamond, quantum devices, quantum sensors, quantum control, noise spectroscopy

1. INTRODUCTION

The practical operation of any quantum device has unavoidably to face the interaction with its environment, which can dramatically limit the device performance by reducing the coherence of the quantum states. Quantum sensing tasks pose a twofold challenge, since the sensor has to be strongly coupled to the external signal to be measured, and meanwhile to be protected against the remaining environment. Here, we consider the task of measuring the amplitude of ultra-weak time-varying magnetic field, in the presence of a noisy environment. This task arises in many practical cases, including *e.g.* the investigation of molecular nano-magnetism, the measurement of neuron and cardiac activity, and more broadly in all the cases where the target signal is a train of impulses, or a multi-frequency signal.

We use a spin qubit sensor based on a single Nitrogen-Vacancy (NV) defect center in standard, commercially available diamond. Thanks to the combination of good optical properties[1] and unprecedented spin properties,[2] the NV center has emerged among solid-state systems as a leading candidate for quantum sensing, offering an unique combination of high sensitivity and high spatial resolution.

In all the applications mentioned above, the parameter estimation task of measuring the signal amplitude of ultraweak fields is challenging. Standard sensor control methods may indeed exhibit sub-optimal performances due to their intrinsic frequency selectivity,[3] which makes the sensor sensitive to only one frequency component of the signal at a given sensing time, and thus leads to the loss of relevant parts of the signal.

We demonstrate how *optimal quantum control*, a valuable tool in quantum computation, can effectively be adapted to tackle the challenge of quantum sensing.[4] We design a new optimization algorithm for quantum sensing, demonstrating better performance than traditional dynamical decoupling control techniques, in terms of

Further author information: fabbri@lens.unifi.it

Quantum Nanophotonic Materials, Devices, and Systems 2019, edited by Cesare Soci, Matthew T. Sheldon, Mario Agio,
Proc. of SPIE Vol. 11091, 110910L · © 2019 SPIE · CCC code: 0277-786X/19/$21 · doi: 10.1117/12.2531734

larger accumulation of the spin phase encoding the field information, and improved protection from environment-induced decoherence.

In this strategy, gaining precise information about the intrinsic noise of the sensor device is also crucial, to build a robust quantum sensor protected by noise-tailored control. We show a protocol for the spectroscopic reconstruction of the noise spectral density (NSD) induced by the complex spin environment of the NV sensor, even when limited by relatively short coherence times.[5] The protocol also distinguishes among classical and quantum coupling regimes, and identifies coherent coupling of the qubit to the local spin environment, thus providing an additional resource to enhance the sensing – or even computational – device performance.[6,7]

2. OPTIMAL QUANTUM CONTROL STRATEGY FOR A QUBIT SENSOR IN NOISY ENVIRONMENT

Optimal quantum control encompasses methods to improve the outcome quality of a quantum process – *e.g.*, efficiently perform a quantum operation, or optimally realize a given quantum state,[8] by designing the optimal time dependence of the driving fields that guides the dynamics of a quantum system. These methods have been successfully applied in a variety of experimental settings, ranging from uncorrelated systems *e.g.* in chemical reactions and molecular processes,[9,10] to single qubits[11] and correlated quantum many-body systems.[12,13] The optimization usually relies on the extremization of some cost function, for example the infidelity of the final state compared to a desired target state,[14] or the final energy excess.[15]

We are here considering the complex sensing task that consists in measuring the amplitude of an ultraweak magnetic field $b(t)$ with multiple frequency components, in a noisy environment. This requires to recast the optimal quantum control strategy. Indeed, without the full knowledge of the external field to be measured – *e.g.*, if one wants to measure the peak amplitude of a propagating action potential – the description of the unitary dynamics of the sensor qubit during the process is not accessible, thus the optimization of the usual fidelity is not feasible. To find the optimal sensor control for quantum sensing, we have thus to introduce a new metric, the sensitivity of the sensor – which also importantly includes the effect of undesired noise sources, unavoidable in practical applications.

The quantum sensor that we use is is the spin qubit associated to an NV center in bulk diamond. We exploit the $S_z = 0, -1$ ground-state electron spin projections of the NV spin triplet as an effective two-level system, in the presence of a static bias magnetic field that removes the degeneracy of the $S_z \pm 1$ spin projections. This spin qubit can be prepared in a well defined initial state, coherently manipulated via magnetic resonance, and read out optically.[16] We apply to the spin qubit different kind of external multitone magnetic field $b(t)$ to be measured, which induces a unitary but unknown spin dynamics. The spin qubit is also coupled to a rich environment, formed by an ensemble of Carbon-13 nuclear spins, present in natural abundance (1%) inside the diamond lattice. This coupling generates additional undesired noise $\beta(t)$, which induces decoherence of the spin qubit. We assume $\beta(t)$ to be described by a stochastic variable with power spectral density $S(\omega)$ in frequency domain, as described in Sec 3.

Control is here applied to the spin qubit via pulsed dynamical decoupling (DD),[18] consisting in series of π pulses that repeatedly flip the spin, thus reversing its temporal evolution. This train of π pulses can be described by a modulation function $y_n(t)$, which has a sign switch at the position of each pulse, indicating the direction of time evolution, forward or backward. A Ramsey interferometer, embedding the control sequences, reads out the phase accumulated by the spin — mapping it into observable population. This phase, due the coupling with the field $b(t)$ during the sensing time T, under the action of the control field, is given by

$$\varphi_n(T) = \int_0^T \gamma\, b(t)\, y_n(t) dt \equiv b\, \phi_n, \tag{1}$$

where $\gamma = 2.81 \times 10^4$ Hz/μT is the NV gyromagnetic ratio. Note that the presence of additional noise $\beta(t)$ imparts random phase shifts during the spin coherent evolution, which leads to a net reduction of the observed population.

Common equispaced DD pulse sequences show high frequency selectivity that can be exploited to measure monochromatic ac magnetic fields,[19] but for this same reason they exhibits suboptimal performances when

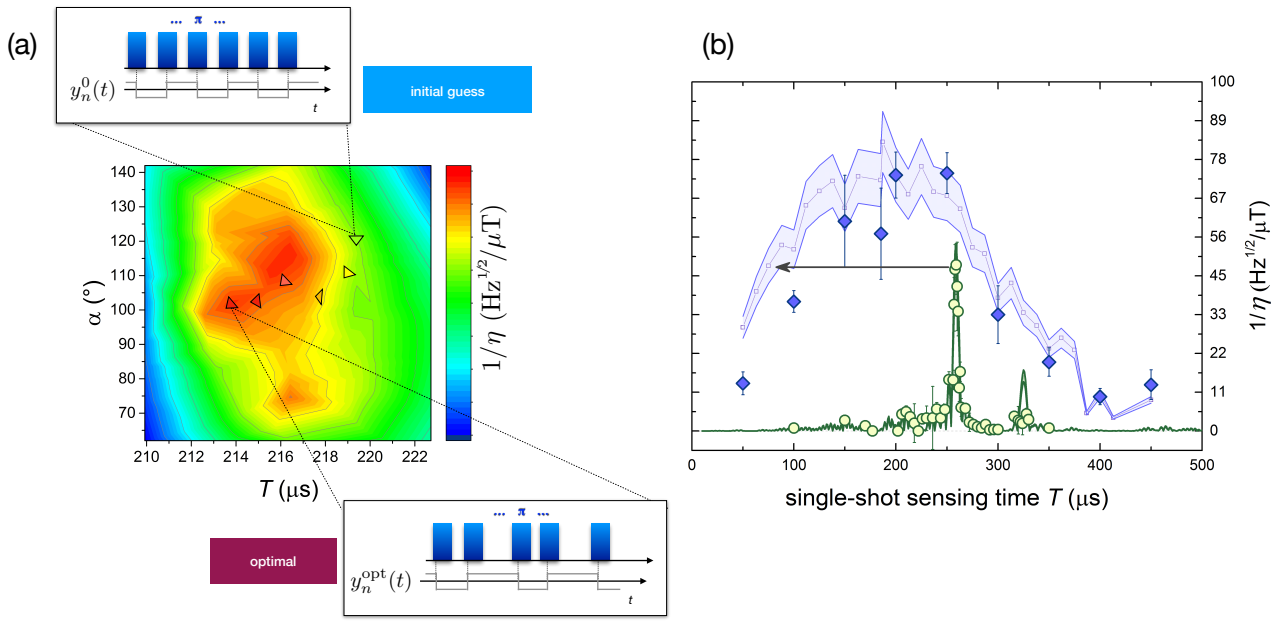

Figure 1. (a) Illustration of the optimization protocol. For the sake of simplicity we show a search in a two-parameter space (sensing time T and phase shift α) for a Carr-Purcell (CP) control sequence[17] used to detect a monochromatic AC field $b(t) = b\cos(2\pi\nu_0 t + \alpha)$, with frequency $\nu_0 = 20.5$ kHz, and unknown amplitude b to be measured. (b) Experimentally measured inverse sensitivity $1/\eta$ in the presence of the field $b(t) = b\sum_i^3 w_i \cos(2\pi\nu_i t + \alpha_i)$, with $\alpha_i = 0$, frequencies $\nu_i = (77; 96; 141)$ kHz and amplitudes $w_i = (0.45; 0.43; 0.12)$ G, under CP (dots) and optimized control (diamonds). The curves represent the theoretical prediction for CP (solid green line) and optimized control (blue line) respectively.

probing multitone target fields, due to unavoidable attenuation of some frequency components. Note that increasing the interrogation time is not advantageous, since it further enhances the sensor frequency selectivity. In addition, each specific temporal dynamics of the target field requires a different sensor control to obtain best performances.

We have thus designed and tested a direct and fast search method that looks for the optimal pulse sequence minimizing the cost function η, that is, sensitivity

$$\eta = e^{\chi_n(T)}\sqrt{t}/|\phi_n(T)|. \tag{2}$$

Remarkably, sensitivity depends on the spin phase $\phi_n(t)$ accumulated during the evolution time T under the unknown field, but also via the decoherence functional, which describes the decay of coherence of the qubit state due to the presence of noise,

$$\chi(T) = \int \frac{d\omega}{\pi\omega^2} S(\omega)|Y_{n,T}(\omega)|^2. \tag{3}$$

where $Y_{n,T}(\omega)$ indicates the the filter control function, squared Fourier transform of $y_n(T)$.

The search is performed by means of a simplex (Nelder Mead) minimization numerical algorithm that allows us to reach global convergence in a multidimensional parameter space (tested up to 51 parameters), as illustrated in Fig. 1a. We analyze which optimization parameters (*e.g.*, total sensing time, π-pulse positions, signal phase, signal trigger time) provide the largest improvement without requiring excessive computational resources. The starting point of the protocol is to choose of an initial guess for the control sequence described by a modulation function $y_n^0(t)$, which depends on a given number of parameters. The algorithm computes the sensitivity η under

the initial control sequence, then produces a number of other trial points $y_n^{(i)}(t)$ and evaluates η for each of them, moving in the multidimensional parameter space, until global convergence is reached. The final point, described by $y_n^{\rm opt}$, represents the optimal control sequence.

An example of optimization for a multitone magnetic field is given in Fig. 1b, showing a remarkable enhancement of sensitivity (blue diamonds) compared to standard control (green dots) when measuring multitone ac fields at fixed interrogation time. In Sec 4 we will consider more extensively the case of a train of gaussian impulses, relevant for applications in biology, physiology, and neuro-science.[20,21]

Note that the described optimal control strategy requires the knowledge of the coherence function $\chi_n(T)$ of the sensor, which affects η (see Eq 2). This in turns depends on the frequency filter $Y_{n,T}(\omega)$ given by the specific sensing sequence, and on the inherent noise that affects the qubit sensor. Thus, a precise knowledge of the NSD $S(\omega)$ appears to be necessary to the successful implementation of the optimization. In the following Section we will describe a protocol that can unravel the characteristics of a complex environment, comprising both unknown coherently coupled quantum systems, and a larger quantum bath that can be modeled as a classical stochastic field.

3. NOISE SPECTROSCOPY OF THE MAGNETIC ENVIRONMENTS

To effectively suppress the effect of unwanted noise, superimposed to the field to be measured, the knowledge of its sources is critical. In this Section, we show a noise spectroscopy protocol[5] that complements the optimal control strategy previously discussed. In the absence of any target field, the NV sensor qubit experiences a rich nuclear spin environment in natural diamond, comprising both coherently coupled quantum systems, and a larger quantum bath that can be modeled as a classical stochastic field $\beta(t)$. To characterize this spin environment, we perform a systematic spectral analysis of the NV coherence under DD sequences of equispaced π pulses with interpulse delay time $2t_1$ [*], where we progressively increase the number of pulses n.[23,24] Due to the presence of the bath, the NV coherence decays as $W(T) = e^{-\chi(T)}$, where $\chi(T)$ depends on the NSD $S(\omega)$, as shown in Eq. 3. For long enough evolution time (*i.e.*, large number of pulses n), equispaced sequences are well described by narrow monochromatic filters given by δ-functions centered at $\omega = \pi/2t_1$, and the coherence decay is expected be exponential,[23] with a characteristic generalized coherence time T_2^L

$$W(nt_1) = \exp\left(-\frac{2nt_1}{T_2^L}\right). \tag{4}$$

An example of this coherence decay is shown in Fig. 2a. The coherence time T_2^L measured for each sequence (at fixed t_1) is primarily affected by the NSD at frequency $\omega = \pi/2t_1$, $S(\omega) \simeq \frac{\pi^2}{8\,T_2^L}$, this approximation being valid for a large number of pulses. However, the coupling with the spin bath leads to a very fast decay ($n < 8$) for t_1 around the first collapse. This induces an artificial broadening on the NSD peak and leads to an incorrect estimate of its maximum amplitude. To overcome the problem of strong decoherence around the Larmor frequency $\omega = \omega_L$ of the nuclear spin bath, we take advantage of the fact that the filter function of an equispaced pulse sequence shows periodic peaks corresponding to different harmonics at $\omega_l = (2l+1)\omega_L$, which indeed affect T_2^L,[23,24]

$$\frac{1}{T_2^L(\omega)} = \frac{8}{\pi^2}\sum_{l=0}^{\infty}\frac{1}{(2l+1)^2}S(\omega_l). \tag{5}$$

This last observation offers a simple tool to overcome the limitation of the short coherence decay time in the collapses time windows. We center the higher order harmonics of the filter function around the expected NSD peak and combine the information from several harmonics. This partially attenuates strong noise that would saturate the coherence decay and achieves a better approximation to a δ-function, as the filter function gets narrower at higher orders for fixed number of pulses. From simulations, we verify that $1/T_2^L$ obtained from the 0^{th}-order filter harmonics ($l = 0$) exhibits significant disagreement with the original spectrum, whereas the $l = 1, 2$ harmonics are sufficient to fully reconstruct the NSD peak. In experiments, we thus extract the NSD lineshape (see blue curve in Fig.2) from a Gaussian fit of $1/T_2^L$ measured around the first and second order collapses (blue dots in Fig. 2), corresponding to the harmonics $l = 1, 2$.

[*]As a base cycle, we use the XY-8 sequence,[22] designed to improve robustness against detuning and imperfections of the π-pulse shape.

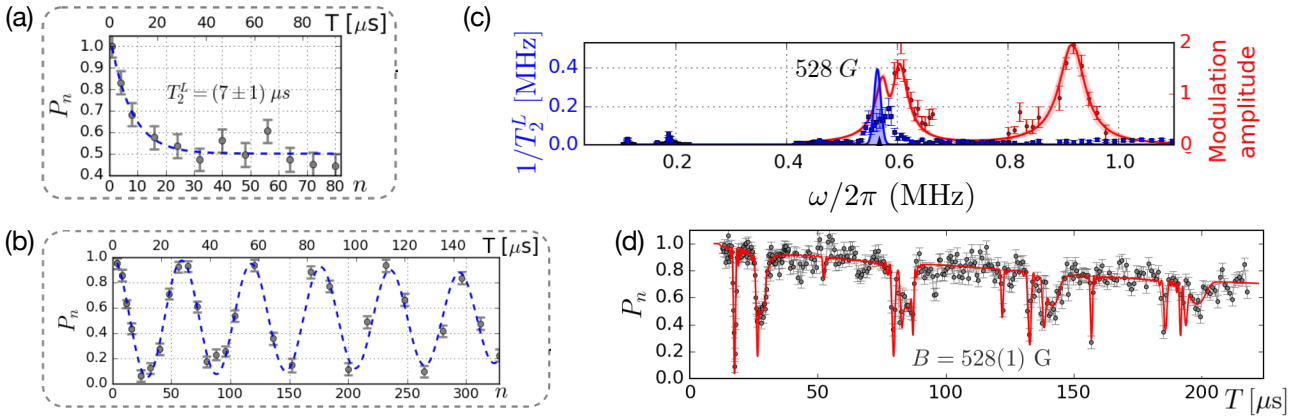

Figure 2. (a)-(b) Spin coherence, mapped onto population P_n, as a function of n. The inter-pulse delay time t_1 is fixed: (a) $t_1 = 242$ ns, $B = 635$ G; (b) $t_1 = 456$ ns, $B = 528$ G. (d) Measurement of the noise spectral density (blue, left-hand side vertical scale) and amplitude of the observed coherent modulations due to the coupling with nearby nuclei. (red, right-hand side vertical scale). Blue lines are the fit of high-order harmonics to extract the noise spectral density, and red lines are the simulations of the completely resolved nearby Carbons (see text). The red shadow describes the uncertainty on the estimation of the coupling strength components. (d) Time evolution of the spin coherence under a DD sequence composed by four repetitions of a XY-8 block[22] (total number of pulses $n = 32$), for a magnetic field strength of $B = 528$ G. Dots are experimental data with statistical error. Red lines are the predicted coherence simulated using the measured environment (see text), with no free parameters.

The reconstruction of the NSD from a classical model fails in some narrow time windows, where the coherence presents sharp dips reaching even negative values ($P_n < 0.5$), as shown in Fig. 2d. The amplitude of these dips show coherent modulation in terms of the number of pulses (for fixed t_1), reflecting the coherent hyperfine interaction with nearby nuclear spins,[25] which can be isolated from noise using equidistant DD sequences. Fig. 2c shows an example of these coherent modulations. Their amplitude shows sharp peaks as a function of frequency (red dots in Fig. 2c), from which we can identify different ^{13}C nuclei and obtain an estimate of the energy-conserving component of the coupling strength, $\omega_h^{||}$.[25] By fitting the modulations with a periodic function calculated using conditional evolution operators (dashed blue line in Fig. 2b), we can also extract a refined estimate of the parallel and orthogonal components of their coupling strength to the NV center (more details are given in Ref.[5]).

Remarkably, noise spectroscopy allows us to mark the boundary between quantum and classical regime. When tuning the bias magnetic field applied along the NV spin, not only the NSD central frequency (corresponding to the ^{13}C Larmor frequency ω_L) is modified, but also the noise properties. As shown in Fig. 3a, the NSD area shows a discontinuity around $B \sim 150$ G, where the interaction energy of most nuclei to the NV spin become comparable with the internal energy of the nuclear bath, $\omega_h^{||} \sim \omega_L$. At higher field ($\omega_h^{||} \ll \omega_L$), the unpolarized nuclear bath is weakly coupled to the NV spin, and can be described as formed by classical randomly oriented magnetic dipoles. The orthogonal component of each nuclear dipole undergoes Larmor precession around the external magnetic field, and the bath can be represented as a classical time-varying mean field with stochastic amplitude and phase, which can be fully characterized by its NSD.

To corroborate the predictive power of the reconstructed environment model – formed by a classical bath and few quantum coherent couplings, we use the acquired information on the NV spin environment to simulate the evolution of the electronic spin for different magnetic fields and under different DD sequences, and we compare the results to corresponding new measurements. At high field, the model successfully predicts the qubit evolution under sequences with non-equidistant pulses. The excellent agreement between data and simulations demonstrates that the spin bath can be described independently of the NV dynamics, since the coupling of the NV center to the spin bath can be neglected compared to the bath internal energy. Figure 3b shows for example

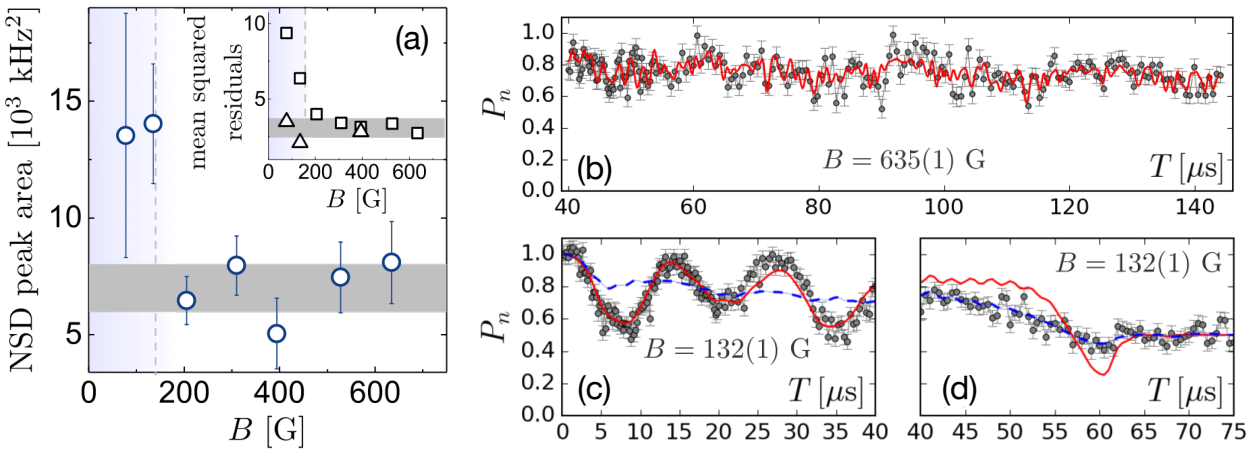

Figure 3. NSD peak area across the quantum-to-classical spin bath transition, obtained from a Gaussian fit of the measured NSD, and reported as a function of the magnetic field strength. The vertical dashed line represents a guide for the eye indicating a sudden change of the bath behavior – where the condition $\omega_h^{||} \sim \omega_L$ for most the ^{13}C nuclei. The gray horizontal region denotes the mean value $\bar{A}$ and the standard deviation σ of the NSD area for $B > 150$ G. Values at field $B \leq 150$ G deviate from $\bar{A}$ by $> 6\,\sigma$. Inset: mean squared residuals of the experimentally observed coherence with the simulation obtained from the measured NSD (squares) and with a 2-model simulation (triangles). Each point results from several datasets collected under different controls. (b)-(d) Time evolution of spin coherence under different DD sequences: UDD with $n = 32$ at high field $B = 635$ G(b), spin-echo (c) and Uhrig $n = 32$ (d) at low field $B = 132$ G. The blue dashed line is obtained from the NSD best fit to a set of multipulse sequences (Uhrig, AXY-4, and AXY-8). Red lines are the predicted coherence simulated using the measured environment, with no free parameters. Inset of (a): Mean squared residuals of the experiments with simulations.

a Uhrig dynamical decoupling sequence (UDD[26]), recently used to detect remote nuclear spin pairs[27] at high field $B = 635(1)$ G. At low field instead, we observe that the NSD measured with equispaced sequences does not predict correctly the measured coherence independently of the applied control (see Fig. 3c and Fig. 3d). One single classical model is no longer suitable to describe the bath when the NV dynamics is driven by different kinds of DD sequences. This can be identified as a the strong-coupling (quantum) regime, where the coupling strength of most nuclei to the NV spin become comparable with the internal energy of the nuclear bath ($\omega_h^{||} \sim \omega_L$, occurring around $B \sim 150$ G). Here indeed we expect the bath dynamics to be modified by the controlled NV dynamics due to the back action of the NV onto the bath itself.

4. A PRACTICAL EXAMPLE: DETECT TRAINS OF GAUSSIAN IMPULSES

Once put in place the optimal control strategy – also thanks to the acquired knowledge of the inherent noise affecting the sensor device – we can apply this strategy to a case study scenario, where the target magnetic field is a train of impulses. This temporal shape applies, *e.g*, to electric and magnetic fields associated with cardiac, neural, and nervous activities of human and animal organs. For the sake of simplicity, we consider a train of gaussian-shaped impulses, with the general form

$$b(t) = b \sum_{i=0}^{m_r} e^{-\frac{(t-i\Delta t)^2}{2\sigma^2}} \tag{6}$$

where $1/\Delta t$ is the repetition rate, and m_r is the number of repetitions, with $m_r\,\Delta t \gg T$. In this case, standard dynamical decoupling may underperform, since the target signal $b(t)$ is positive-defined in the whole temporal domain, thus the product $y_n(t)b(t)$ may be alternately positive and negative, reducing the accumulation of useful phase (see Eq. 1). In other words, each time a π-pulse reverses the spin dynamics, it can partially cancel not only the effect of unwanted noise, but also the phase associated to the field to be measured.

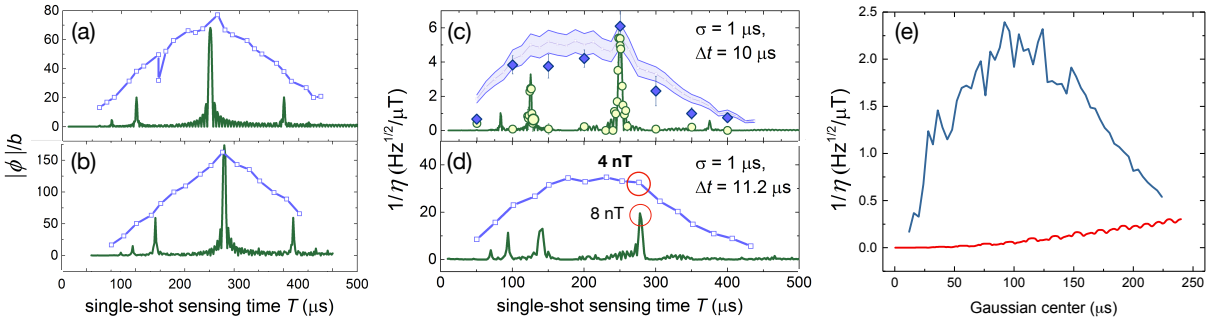

Figure 4. (a)-(d) Optimization of the control for sensing a train of gaussian impulses of width σ and repetition rate $1/\Delta t$: Modulus of the phase accumulated by the spin qubit sensor in the presence of the target field (panels (a) and (b)), and the inverse of sensitivity $1/\eta$ (panels (c) and (d)), as a function of the sensing time T, under CP-50 control (green solid curves) and under optimized control (blue lines with squares) with interpulse delay time in the interval $(0.6 - 10)$ μs. (e) Optimization for a slow gaussian impulse: Inverse of sensitivity for a CP sequence (red), and for an optimal control sequence (blue), with optimized interpulse time intervals, $n = 8$.

For a train of short gaussian impulses, as shown in Fig. 4(a)-(d), optimal control (in blue) outperforms CP (in green) both in the phase accumulated due to $b(t)$, and in sensitivity η, over a large sensing time range. Both CP and optimal control do lead to their largest phase accumulation when $T \simeq n\Delta t/2$, where they give similar results in ϕ_n. This condition corresponds of having couples of π-pulses located in each "empty" time window between two gaussian pulses of the target field, albeit optimal control corrects in a non-trivial way the distribution of π-pulse positions to minimize η. Thus, the π pulses partially reverse the spin qubit dynamics due to undesired noise, but do not cancel the phase due to the target field $b(t)$. We also note that, even when the phase accumulated with CP and with optimal control is comparable, optimal control compensates better than CP for decoherence, leading to better overall sensitivity. This seems to indicate that numerically optimized sequences might be useful also for other quantum information tasks, such as building a robust memory. When measuring slowly-varying fields, such as the slow temporal profile given by a single broad gaussian pulse with $\sigma = 150$ μs, the optimized method performs even better, as shown in Fig. 4(e).

5. CONCLUSIONS

We have devised a versatile and robust method for quantum metrology with a single qubit, based on *optimal quantum control*. We have demonstrated its operation and the advantage it bestows in the measurement of weak time-varying magnetic fields with a NV spin sensor in noisy environments. Complementarily, we have also experimentally demonstrated a method to spectrally characterize the nuclear spin environment of NV centers, even when the resulting NV coherence time is short. The presented strategy may find broad applications in the face of the increasing requirements for NV spin sensors, and it can be also applied to devices based on other physical platforms.

ACKNOWLEDGMENTS

This work was supported by European Research Council through Starting Grant Q-SEnS2 (No. 337135), and NSF Grant No. EECS1702716.

REFERENCES

[1] I. Aharonovich and E. Neu, "Diamond Nanophotonics," *Advanced Optical Materials* **2**, pp. 911–928, July 2014.

[2] N. Bar-Gill, L. M. Pham, A. Jarmola, D. Budker, and R. L. Walsworth, "Solid-state electronic spin coherence time approaching one second," *Nature Communications* **4**, pp. 1743–6, 1.

[3] C. L. Degen, F. Reinhard, and P. Cappellaro, "Quantum sensing," *Rev. Mod. Phys.* **89**, p. 035002, Jul 2017.

[4] F. Poggiali, P. Cappellaro, and N. Fabbri, "Optimal Control for One-Qubit Quantum Sensing," *Physical Review X* **8**, p. 021059, June 2018.

[5] S. Hernández-Gómez, F. Poggiali, P. Cappellaro, and N. Fabbri, "Noise spectroscopy of a quantum-classical environment with a diamond qubit," pp. 1–6, Dec. 2018.

[6] G. Goldstein, P. Cappellaro, J. R. Maze, J. S. Hodges, L. Jiang, A. S. Sorensen, and M. D. Lukin, "Environment assisted precision measurement," *Phys. Rev. Lett.* **106**(14), p. 140502, 2011.

[7] M. H. Abobeih, J. Cramer, M. A. Bakker, N. Kalb, M. Markham, D. J. Twitchen, and T. H. Taminiau, "One-second coherence for a single electron spin coupled to a multi-qubit nuclear-spin environment," *Nature Communications* **9**(2552), 2018.

[8] S. J. Glaser, U. Boscain, T. Calarco, C. P. Koch, W. Koeckenberger, R. Kosloff, I. Kuprov, B. Luy, S. Schirmer, T. Schulte-Herbrueggen, D. Sugny, and F. K. Wilhelm, "Training Schrödinger's cat: quantum optimal control," *The European Physical Journal D* **69**(12), p. 279, 2015.

[9] D. J. Tannor and S. A. Rice, "Control of selectivity of chemical reaction via control of wave packet evolution," *J. Chem. Phys.* **83**, pp. 5013–5018, Nov. 1985.

[10] P. Brumer and M. Shapiro, "Laser control of molecular processes," *Annual Review of Physical Chemistry* **43**, pp. 257–282, Oct. 1992.

[11] J. Scheuer, X. Kong, R. S. Said, J. Chen, A. Kurz, L. Marseglia, J. Du, P. R. Hemmer, S. Montangero, T. Calarco, B. Naydenov, and F. Jelezko, "Precise qubit control beyond the rotating wave approximation," *New J. Phys.* **16**(9), p. 093022, 2014.

[12] S. Rosi, A. Bernard, N. Fabbri, L. Fallani, C. Fort, M. Inguscio, T. Calarco, and S. Montangero, "Fast closed-loop optimal control of ultracold atoms in an optical lattice," *Physical Review A* **88**, p. 021601, Aug. 2013.

[13] M. G. Bason, M. Viteau, N. Malossi, P. Huillery, E. Arimondo, D. Ciampini, R. Fazio, V. Giovannetti, R. Mannella, and O. Morsch, "High-fidelity quantum driving," *Nat Phys* **8**, pp. 147–152, Feb. 2012.

[14] T. Caneva, T. Calarco, and S. Montangero, "Chopped random-basis quantum optimization," *Phys. Rev. A* **84**, p. 022326, Aug 2011.

[15] P. Doria, T. Calarco, and S. Montangero, "Optimal control technique for many-body quantum dynamics," *Phys. Rev. Lett.* **106**, p. 190501, May 2011.

[16] M. W. Doherty, N. B. Manson, P. Delaney, F. Jelezko, J. Wrachtrup, and L. C. Hollenberg, "The nitrogen-vacancy colour centre in diamond," *Physics Reports* **528**(1), pp. 1 – 45, 2013.

[17] H. Y. Carr and E. M. Purcell, "Effects of diffusion on free precession in nuclear magnetic resonance experiments," *Phys. Rev.* **94**(3), pp. 630–638, 1954.

[18] L. Viola and S. Lloyd, "Dynamical suppression of decoherence in two-state quantum systems," *Phys. Rev. A* **58**, p. 2733, 1998.

[19] J. M. Taylor, P. Cappellaro, L. Childress, L. Jiang, D. Budker, P. R. Hemmer, A. Yacoby, R. Walsworth, and M. D. Lukin, "High-sensitivity diamond magnetometer with nanoscale resolution," *Nat. Phys.* **4**(10), pp. 810–816, 2008.

[20] J. Wikswo, J. Barach, and J. Freeman, "Magnetic field of a nerve impulse: first measurements," *Science* **208**, pp. 53–55, Apr. 1980.

[21] G. Bison, N. Castagna, A. Hofer, P. Knowles, J.-L. Schenker, M. Kasprzak, H. Saudan, and A. Weis, "A room temperature 19-channel magnetic field mapping device for cardiac signals," *Applied Physics Letters* .

[22] T. Gullion, D. B. Baker, and M. S. Conradi, "New, compensated carr-purcell sequences," *J. Mag. Res.* **89**(3), pp. 479 – 484, 1990.

[23] T. Yuge, S. Sasaki, and Y. Hirayama, "Measurement of the noise spectrum using a multiple-pulse sequence," *Phys. Rev. Lett.* **107**, p. 170504, Oct 2011.

[24] G. A. Álvarez and D. Suter, "Measuring the spectrum of colored noise by dynamical decoupling," *Phys. Rev. Lett.* **107**, p. 230501, 2011.

[25] T. H. Taminiau, J. J. T. Wagenaar, T. van der Sar, F. Jelezko, V. V. Dobrovitski, and R. Hanson, "Detection and control of individual nuclear spins using a weakly coupled electron spin," *Phys. Rev. Lett.* **109**, p. 137602, Sept. 2012.

[26] G. S. Uhrig, "Keeping a quantum bit alive by optimized π-pulse sequences," *Phys. Rev. Lett.* **98**, p. 100504, Mar 2007.

[27] N. Zhao, J.-L. Hu, S.-W. Ho, J. T. K. Wan, and R. B. Liu, "Atomic-scale magnetometry of distant nuclear spin clusters via nitrogen-vacancy spin in diamond," pp. 1–5, Mar. 2011.